Germanium Nanowires-in-Graphite Tubes *via* Self-Catalyzed Synergetic Confined Growth and Shell-Splitting Enhanced Li-Storage Performance

Yong Sun, Shuaixing Jin, Guowei Yang, Jing Wang, and Chengxin Wang*

State Key Laboratory of Optoelectronic Materials and Technologies, The Key Laboratory of Low-Carbon Chemistry & Energy Conservation of Guangdong Province, School of Physics Science and Engineering, Sun Yat-sen (Zhongshan) University, Guangzhou 510275, People's Republic of China

ABSTRACT Despite the high theoretical capacity, pure Ge has various difficulties such as significant volume expansion and electron and Li^+ transfer problems, when applied as anode materials in lithium ion battery (LIB), for which the solution would finally rely on rational design like advanced structures and available hybrid. Here in this work, we report a one-step synthesis of Ge nanowires-in-graphite tubes (GNIGTs) with the liquid Ge/C synergetic confined growth method. The structure exhibits impressing LIB behavior in terms of both cyclic stability and rate performance. We found the semiclosed graphite shell with thickness of ~50 layers experience an interesting splitting process that was driven by electrolyte diffusion, which occurs before the Ge–Li alloying plateau begins. Two types of different splitting mechanism addressed as "inside-out"/zipper effect and "outside-in" dominate this process, which are resulted from the SEI layer growing longitudinally along the Ge–graphite interface and the lateral diffusion of Li^+ across the shell, respectively. The former mechanism is the predominant way driving the initial shell to split, which behaves like a zipper with SEI layer as invisible puller. After repeated Li^+ insertion/exaction, the GNIGTs configuration is finally reconstructed by forming Ge nanowires–thin graphite strip hybrid, both of which are in close contact, resulting in enormous enchantment to the electrons/Li^+ transport. These features make the structures perform well as anode material in LIB. We believe both the progress in 1D assembly and the structure evolution of this Ge–C composite would contribute to the design of advanced LIB anode materials.

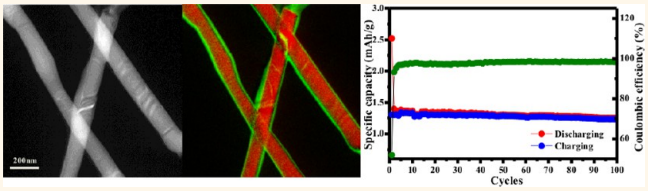

KEYWORDS: Ge nanowires · graphite tubes · core–shell · self-catalyzed growth · lithium ion battery

Recently, Ge has been considered as a promising anode material in LIB, offering an alternative to graphite due to its excellent lithium diffusivity and high theoretical capacity (approximately 1600 mAh/g), which is second only to Si (approximately 4200 mAh/g) among all Li-alloying materials.[1−6] However, such high capacity has never been utilized completely due to the capacity fading and bad rate performance resulted from pronounced volume expansion (>300% volume change for fully lithiated Ge) and pulverization problems. On the other hand, enhancing Li^+ and electron transport is another critical point. All of these difficulties must be solved, if Ge applied as anode materials are to meet the increasing claim for high-performance LIB.[7−10] In this situation, available structural design such as low-dimensional nanostructures fabrication and rational hybrids is very necessary. Recently, an active anode material in combination with various forms of carbon has been extensively pursued to improve cyclic stability and rate performance.[11−18] The advantages of carbon as an additional component in electrodes originate from its ability to help transport Li^+/electrons and resist massive volume changes, which provides compensation for pure working materials. In this manner, a lot of works about Ge micro-nanoparticles encapsulated with amorphous carbon emerge recently, reporting the improved Li-storage performance.[19−26] For 1D core–shell nanostructures, the Ge–C combination has drawn wide attention in past years even beyond the Li-storage field, which provides an interesting strategy contributing to semiconductor field with

* Address correspondence to wchengx@mail.sysu.edu.cn.

Received for review December 5, 2014 and accepted March 4, 2015.

Published online March 04, 2015
10.1021/nn506955f

carbon shell serving as antioxidation layer. Approaches based on VLS growth and two-step process were developed to prepare carbon encapsulated Ge nanowires. For instance, P. D. Yang *et al.* have done it by subjecting Ge nanowires to a thermal treatment in an organic vapor doped vacuum.[27] E. Sutter *et al.* demonstrated a route that can encapsulate a ready-made Ge nanowire with carbon shell through an *in situ* annealing process under TEM.[28] Recently, another stimulation of efforts was devoted to the rational combination of Ge nanowires and carbon layer based on the purpose of advanced LIB anode materials. Significantly, Cho *et al.* reported the Ge nanowires sheathed with amorphous carbon *via* a solid−liquid approach and investigated its behavior as LIB anode material.[29] Yu *et al.* synthesized fully and homogeneously carbon-encapsulated Ge and GeOx nanowires by a one-step process. Both of the resulted Ge/C and the GeOx/C nanowires exhibited improved performance.[30] Moreover, Choi *et al.* endowed Ge nanowires with an excellent cycle stability and rate performance by growing a few layers of graphene on the surface with a two-step procedure.[31]

Nevertheless, it seems that fabrication of high-quality Ge−C 1D noncables simply in large amount still remains a great challenge by now. Novel GIGNTs configuration as LIB anode has never been investigated before, leaving several interesting points unclear. For example, it is usually recognized that the thick carbon shell in the form of graphite layer would prevent Li^+ from diffusing across the van der Waals bonded close C−C 2D planes. Additionally, the sharply adjacent core and shell would fail to resist the internal expansion, because there is no buffer space between the active nanowire and the graphite layer. In this manner, it was thought to be not really a good idea to encapsulate the nanowire closely with a thick graphite shell for LIB materials. However, elaborative investigation about what has a core−shell experienced accompanying the electrochemical lithiation is rare to see. The interaction between a ∼50 layers of graphite shell and the nanowire core during repeated intercalation/deintercalation processes remains unknown, raising the following questions: (1) Do the graphite layers prevent Li^+ from contacting the electrode and how it occurs? (2) If not, how would the shell evolve against the core expansion? (3) What is the influence on subsequent cycles, positive or negative? All of these items deserve to be clarified.

Here in this work, we demonstrate first a novel strategy to achieve GNIGTs that is based on the fact that Ge−C is noneutectic in moderate conditions, suggesting the possibility for the heterogeneous and simultaneous growth of double phases through rational control. By creating a liquid/solid interface between Ge and C, we achieved core−shell nanostructures of GNIGTs *via* synergetic confined growth in a one-step CVD (chemical vapor deposition) process using GeO_2 and CH_4. Interestingly, the prepared GNIGNs delivers excellent performance both in cycle stability and rate test when applied as LIB anode material. Systematic *ex situ* experiments relying on HRTEM and EELS were employed to investigate the morphology evolution along with the alloying expansion. It is found that Li^+ can not only diffuse freely along the interface between the Ge nanowires and carbon tubes, but penetrate across the graphite wall laterally through the defect sites. The lithiation expansion resulted splitting of the shell would facilitate the reconstruction of new Ge−C composites. Systematic investigation and analysis was carried out with appropriate models built to demonstrate the interesting topics proposed above.

RESULTS AND DISCUSSION

The as-synthesized product is shown in Figure 1, in which (a) is a scanning electron microscope (SEM) image and the inset is the corresponding X-ray diffraction (XRD) pattern that confirms the presence of cubic Ge (PDF # 65−0333) nanowires. A typical single Ge nanowire is inserted into a semiclosed graphite tubes, the open end of which is shown in Figure 1(c). Figure 1(b) provides a closer view of these nanowires, in which the distinct contrast difference resulting from different atomic weights represents the graphite shell and Ge nanowire core. Figure 1(h) is an SAED (selected area electron diffraction) pattern corresponding to Ge components, which is consistent with the phase established by XRD characterization. Figure 1(f) is a high resolution transmission electron microscopy (HRTEM) image of a single nanowire. Each Ge nanowire core is wrapped by a graphite shell with a thickness of approximately 20 nm. Further elemental analyses by EELS (Electron energy loss spectroscopy) mapping and energy diffraction spectrum (EDS) line scanning as shown in Figure 1(g,i) prove the existence of a GNIGT hybrid structure. The Ge cores are often cracked, resulting in hollow tubes in some of the nanowires shown in Figure 1(b), which implies the noneutectic effect at the interface between Ge and C.

The formation of the GNIGTs core−shell nanostructure in a one-step process originates from synergetic confined growth at the noneutectic interface, as illustrated in Figure 2. As the temperature increase, GeO_2 would be reduced to GeO and Ge by H_2 at about 700 °C, which result in the evaporation and transport of Ge source. The transported Ge clusters would absorb carbon atoms that remain on the surface, forming a sharp heterogeneous interface due to the Ge−C noneutectic effect in a moderate quasi-equilibrium state. In the following ∼10 min, the temperature would increase above 1000 °C that was higher than the melting point of Ge. The Ge−C clusters in the atmosphere would aggregate and form novel configuration that liquid Ge drops are wrapped by floating C shell, as

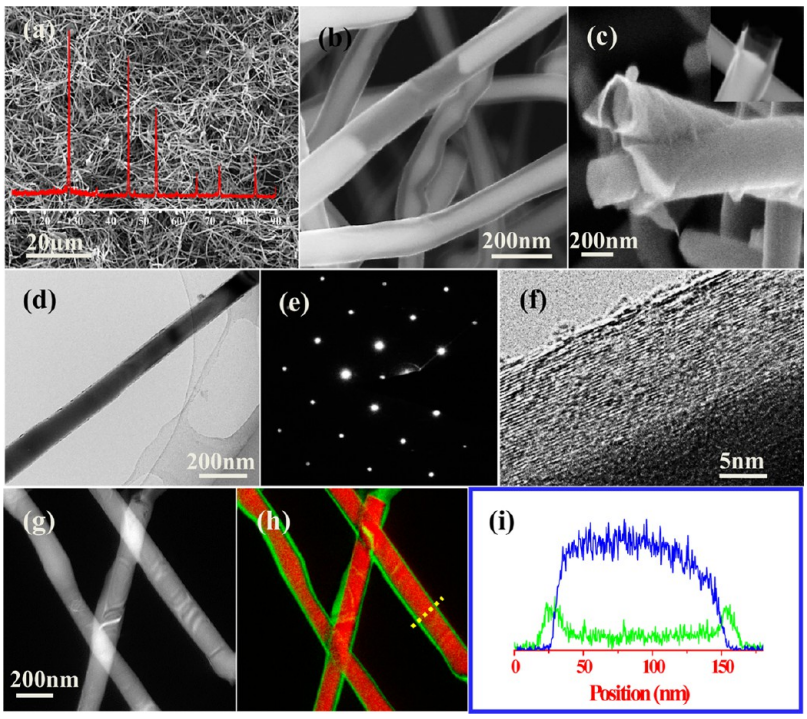

Figure 1. Morphology, structure and elemental characterization of GNIGTs. (a) The typical low-magnification SEM image of the sample; the red curve as the inset is the corresponding XRD pattern. (b) A closer view of the core−shell configuration; the bright and dark cantrast in a 1D structures point to Ge cores and carbon shells. (c) The inset is the open end of the Graphite tubes in different perspectives. (d) The bright field image of a single unite under TEM. (e,f) The SAED pattern and the HRTEM image of the nanowire. (g) The low-magnification dark-field TEM image of several nanowires. (h) EELS mapping result of nanowires shown in (g); the green shell and the red core represent carbon and Ge respectively. (i) EDS elemental line scanning along the yellow path in (h).

denoted by "I" in Figure 2. the solid−liquid hybrid serves as dynamic units that allow Ge cores to grow larger, benefiting from the continuous resource supply, and allow the shell to become ordered graphite layers if the C shell is sufficiently thick at the local scale. As soon as graphite layers form, they act as local barriers that confine liquid Ge. However, the liquid would penetrate out through a thinner coating or defect-rich region due to the asymmetric surficial strain tolerance and then cause larger gaps, denoted as "II" in Figure 2. The exposed liquids enhanced the absorption of additional C and Ge clusters, assembled as extended quasi-1D core−shell nanostructures and denoted as step "III". Repetitions of "II" and "III" finally result in 1D GNIGTs nanostructures, denoted as "IV". This non-eutectic solid/liquid interface-enhanced, synergetic, and confined model accounts for the semiclosed nature of CNTs shells as well as the closed end wrapping a knob that is commonly observed in SEM and TEM images. In Figure 2, SEM images corresponding to the different growth steps are provided to enhance the graphic illustration. We determined the growth steps by preventing the smooth growth process through lowering the target temperature and reducing the reaction time. In Figure 2, the open and closed ends of semiclosed graphite tubes are marked as green and red arrows, respectively.

This synergetic confined growth is feasible in not only the Ge−C system but also other metal-C non-eutectic cases as long as the metal has a suitable melting point and thermal transport kinetics. The above parameters are required to ensure the coexistence of metallic clusters CH_4-derived C on a long time scale in the atmosphere. A GeO_2 source whose melting point is at approximately 1115 °C would be largely reduced to Ge at this temperature by reduced matter. At the same time, the cracking temperature of CH_4 in an H_2 environment is approximately 1000 °C. The forming Ge clusters with a melting point of approximately 938 °C are not easily pulled away by gas flow but remain in the atmosphere. Both of the requirements enhance the above growth mechanism. To confirm our proposal, Cu, with a melting point of 1084 °C, was chosen to achieve Cu nanowires-in-graphite tubes guided by the above method after rational design. In this experiment, Cu powder, CH_4, and H_2 were used as resources and carrier gas. To create a Cu liquid drop at the same region on a ceramic chip, the reaction temperature was increased to 1250 °C because of the higher melting point. The morphological and TEM characterization of the product are shown in Figure S1 (Supporting Information), in which electrons energy loss spectrum (EELS) elemental mapping and HRTEM analysis confirm the Cu nanowires-in-graphite tubes configuration.

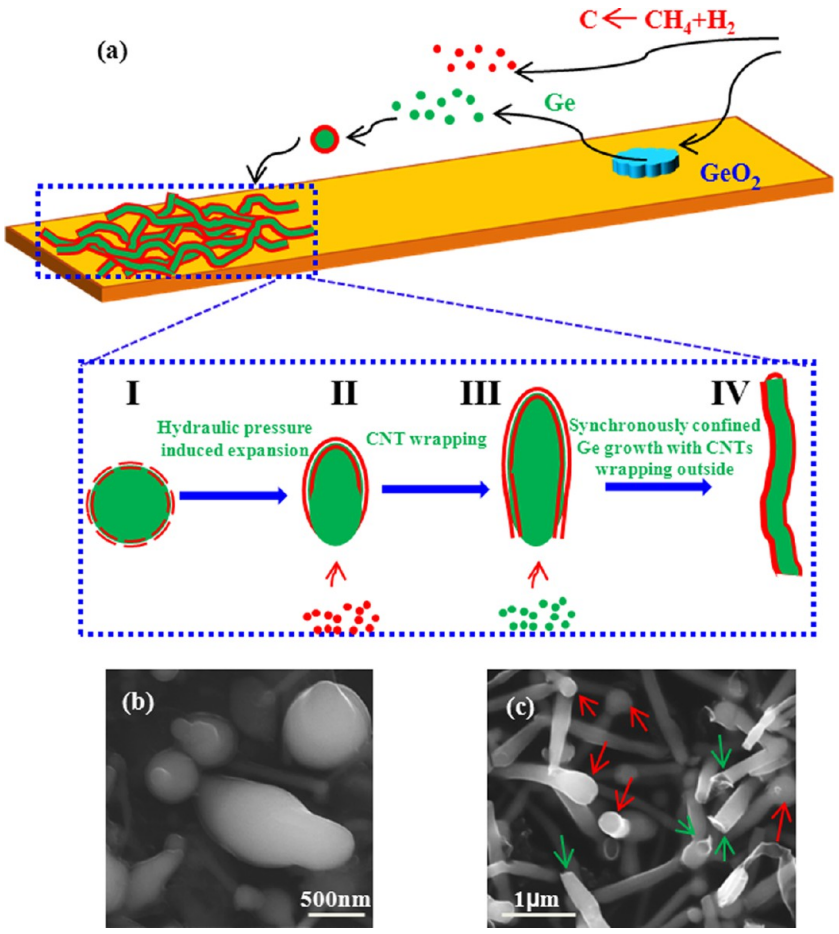

Figure 2. Illustration of the synergetic-confine-growth of Ge nanowires @ Graphite tubes. (a) The upper section guided by thin black arrows demonstrates the source transport, as well as the precursor location and the product deposition region on the ceramic sheet; the down section in dotted square illustrate the self-assembly process of a GNIGT nanostructure. (b) The morphology of product at step I and II that resulted from the unsmooth growth. (c) The SEM image of the product that experienced a smooth growth, corresponding to step III and IV.

As shown in (a), the morphology is not exactly the same as that of GNIGT; several 1D structures tend to clump together in a large Cu sphere, which reflects the difference in physical features between Ge and Cu, such as the melting point, the atomic weight, and even the surficial energy of the liquid drop. These physical differences result in different transport and liquid kinetics. The growth of most nanostructures proceeds to step II and then ceases due to a shortage of Cu resources. Although a high-quality and uniform 1D nanostructure was not obtained, the present results are compliant with the assembly mechanism proposed in GNIGTs.

In the proposed model, the growth of a high-quality product relies on the control of CH_4 partial pressure. A synthetic investigation of the relationship between the proportion of CH_4 and the product structures was performed. In this serial experiment, the initial atmosphere was composed of CH_4 and H_2, in which the proportion of CH_4 was 10, 20, and 50%, with the other conditions remaining the same. The morphological and structural characterizations of the three samples are presented in Figure S2, in which panels (a), (b), and (c) correspond to the different CH_4 proportions. As expected, the three conditions result in graphite layers with different thicknesses. Notably, as the CH_4 proportion increases, the diameter of Ge cores become thinner and the product yield decreased. An excessive C resource such as a 50% CH_4 ratio, which generates thicker graphite layers, would hinder Ge nanowires propagated in the lateral direction by influencing the Ge supply in step **I**. At the same time, small Ge clusters wrapped by the C layer would be transported away without deposition, leaving fewer products than lower CH_4 proportions (*e.g.*, 10%). The Raman spectra of the three samples are displayed in Figure S2(d), in which the intensity ratio difference between C and Ge signals can be distinguished, implying different C shell thicknesses.

This novel structure would be advantageous over conventional materials if assembled as an anode material in an LIB device because the graphite shell helps to not only dredge the electron-transporting path but also maintain the integrity of the intact

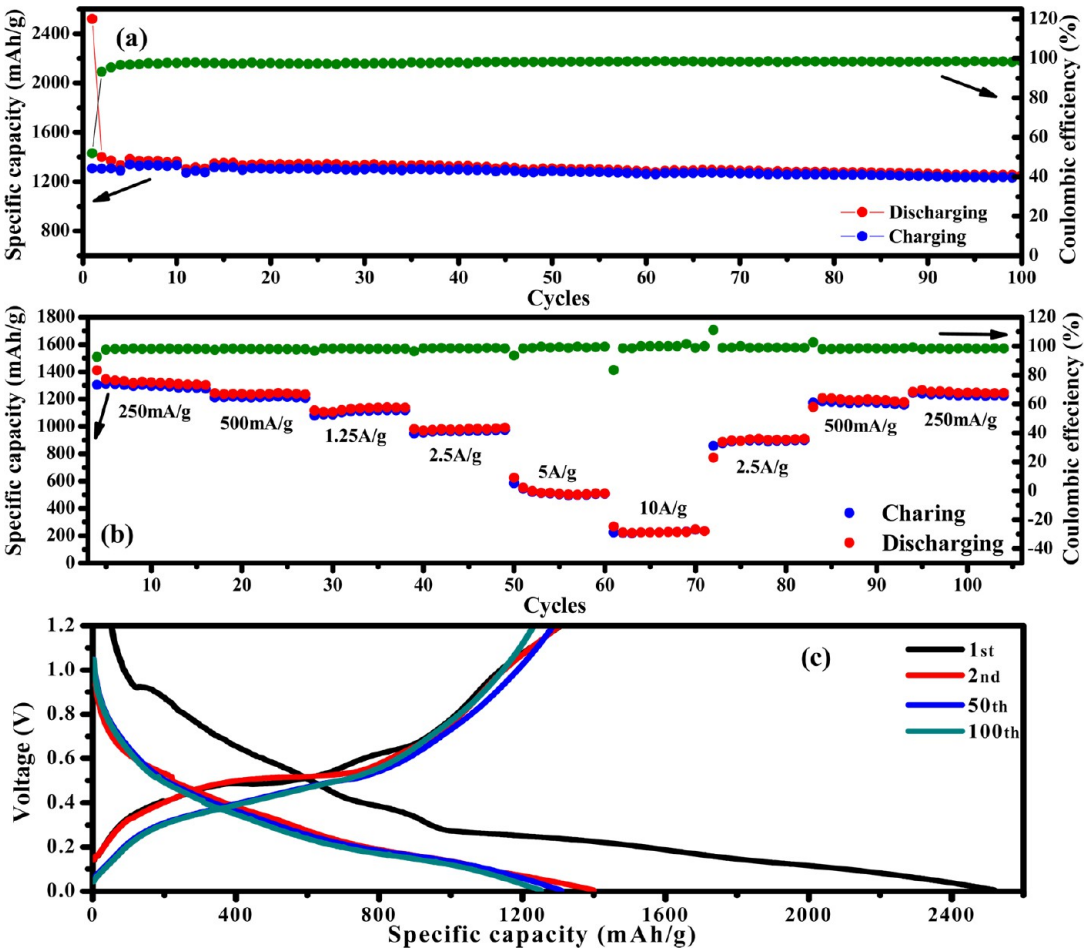

Figure 3. LIB cyclic stability test and rate performance of the composite. (a) 100 cycles' capacity measurement; (b) rate performance test at the rates of 250 mA/g to 10A/g; (c) specific capacity−voltage curves of the 1st, 2nd, 50th and 100th cycles.

one-dimensional (1D) profile against volume expansion during the lithiation process. Herein, the detailed LIB performance in a half cell was investigated, and related electrochemical characterizations were performed. The galvanostatic charge/discharge tests used a current density of 250 mAh/g in the potential range of 0.005−1.2 V *vs* Li^+/Li. The specific capacity was calculated based on the total mass of the Ge nanowire and graphite tube shell composite. Typical potential-capacity curves at the 1st, 2nd, 50th, and 100th cycles are provided in Figure 3(c), from which the GNIGTs delivers a capacity of 2503, 1396, 1314 and 1241 mAh/g, respectively. The value of 2503 mAh/g that is much higher than the theoretical capacity of pure Ge (1600 mAh/g) indicates there is high irreversible capacity. As would be shown later, the graphite shell of a GNIGT would split after the first charging process. SEI layer would form on the surface of both Ge nanowire and graphite layer. The dissilient graphite tube would be further stripped into thinner units due to lithiation expansion, which results in an extra interface with the electrolyte. All of these factors are responsible to the high initial capacity loss and irreversible capacity. The retention of the charge/discharge curves at the 100th cycle, shown in Figure 3(a), demonstrates the excellent cyclic stability of the composite as an anode material. The reversible specific capacity exhibits stable evolution, which maintains approximately 88.9% of the second capacity after 100 cycles. The abrupt leap at the 11th and 14th cycles is attributed to the environmental temperature change during the measurement. Under stable test conditions, the coincidence between charge and corresponding discharge capacity demonstrating a stable Coulombic efficiency of approximately 99%, indicates the high reversibility of the anode material.

To further manifest the outstanding performance, the rate capability was also evaluated by applying various current densities ranging from 0.25 to 10 A/g, as shown in Figure 3(b). The GNIGTs anode exhibits high reversible capacities of approximately 1310, 1240, 1130, 982, 515, and 232 mAh/g at current densities of 0.25, 0.5, 1.25, 2.5, 5, and 10 A/g, respectively, in the rate-increasing procedure. The capacity at a current density of 5 A/g is considerably higher than the theoretical capacity of commercial graphite anode material (372 mAh/g). After more than 70 cycles at various rates, when the current density returned stepwise

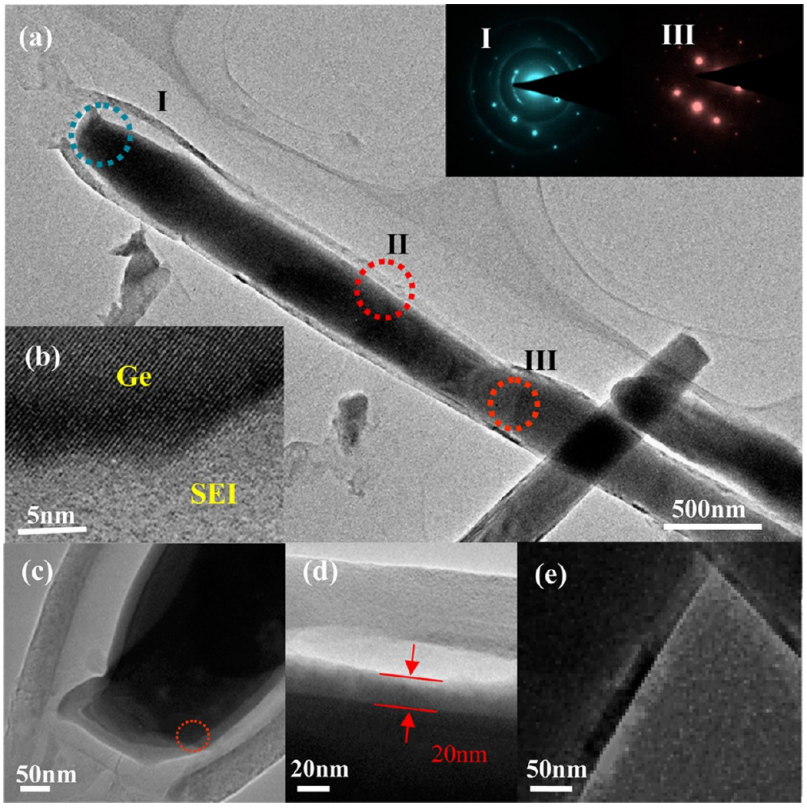

Figure 4. Morphology and structure analysis of an incomplete splitting GNIGT. (a) The single nanowire that was used for analysis; the insets I and III are SAED patterns corresponding to the areas marked in the image. (b) The HRTEM image of the red circle area in (c), which clearly displays the boundary of Ge core and SEI layer. (c−e) The closer view of the edge parts of I, II and III regions; the interface of Ge−C in I/II regions is separated by SEI layer, while there is no obvious change in "III" area.

to 0.25 A/g, the reversible capacities recovered to approximately 915, 1185, and 1241 mAh/g at 0.25, 0.5, and 2.5 A/g, respectively, which are close to the previous values.

Such an impressed performance is inextricably related to the particular configuration of GNIGTs, which might be ruled by an advantageous structure evolution mechanism. In order to shed light on this interesting topic, systematic experiments and analysis was done to investigate the morphology evolution of the novel structure as Li^+ insertion/extraction. We highlight the items like the interaction between the carbon shell and the Ge nanowire, as well as the resulted consequence on the cyclicity. *Ex situ* TEM analysis was employed frequently to observe the morphology change. It is found two types of kinetic mechanism refereed as "outside-in" and "inside-out" dominates the shell splitting, as denoted from Figure 4 to Figure 6. For TEM observation, the first discharge process was halted at 0.35 V, which can expose the kinetic image of the Li^+ insertion path and the preliminary morphology evolution. Figure 4 exhibits the typical morphology of single nanowire at this stage that indicates the "inside-out" splitting mechanism. It is induced by the rapid Li^+ diffusion along the inside walls of CNTs, which begins at the open end. In fact, this process enhances the growth of SEI film on the interface of Ge nanowire and graphite shell as soon as the joint is unzipped, as shown in Figure 4(a). Both of the Li^+ insertion and the increasing thickness of the film drive the radial expansion of the core and then impose an external inside-out force against the inner wall of the CNTs, which finally resulted in the cleavage of the shell. Noticeably, this reaction proceeds along the 1D nanostructure longitudinally until the coaxial shell split completely. Since the TEM analysis was applied *ex situ*, it is worthy to exclude the possibility that the layer formed due to surficial oxidation of Ge core. We did a couple of comparative experiments as shown in Figure S4 and Figure S5, which correspond to the sample without any treatment and after being soaked in diethyl carbonate for 1 week, respectively. These data imply that the layer can form and be removed without being exposed to air. The evolution kinetics mentioned above can be demonstrated further by the evidence shown as Figure 4(c−e), which presents the closer view corresponding to the regions "I", "II" and "III" in Figure 4(a), respectively. From Figure 4(c,d), the thickness of the interface layer is about 20 nm. Figure 4(b) is the HRTEM image of the marked area in Figure 4(c), which displays a single-crystal Ge body. Noticeably, the edge of the Ge core shown as Figure 4(b) is not as smooth as the initial Ge nanowires. Both of the facts indicate the Ge part was etched at the interface and the Ge−Li reaction has

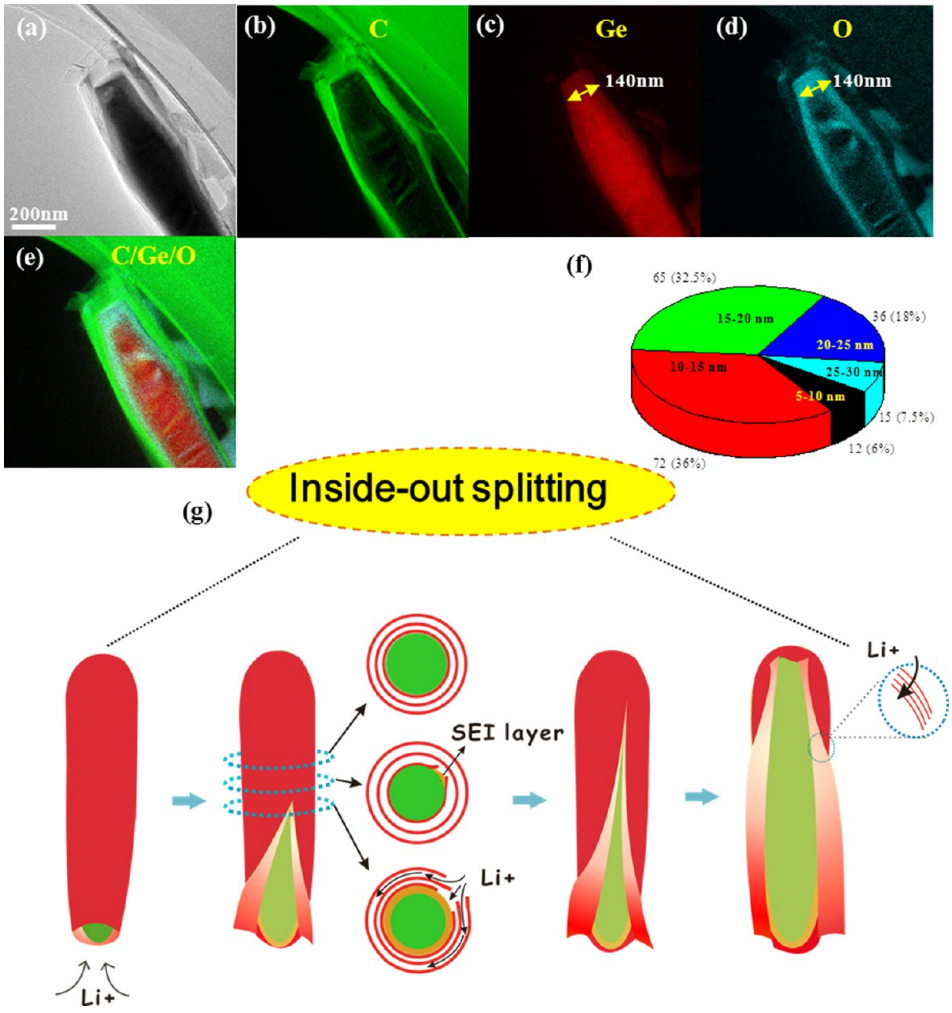

Figure 5. Elemental analysis of an incomplete splitting GNIGT with diameter less than 200 nm and the proposed shell splitting model. (a) The bright-field TEM image of the nanowire used for analysis. (b–d) The EELS elemental mapping of C, Ge and O. (e) The C/Ge/O elements overlap image. (f) The thickness statistics of C shells that collected among ~200 GNIGTs used for LIB test. (g) The illustration of the proposed inside-out splitting mechanism of a graphite shell. The origin of the splitting can be demonstrated by interfacial lithiation/expansion and SEI layer forming, both of which together act as invisible puller for the unzipped effect upon a carbon shell. In this process, SEI layer would form on surface of Ge part as soon as it is in touch with electrolyte.

not occurred in inner part. Figure 4(d) points to the reaction front along the nanowire, and Figure 4(e) displays the area that is intact from Li^+ insertion, in which the carbon shell still keep in close touch with the Ge nanowire. The insets are the SAED (selected area electron diffraction) patterns corresponding to the region "I" and "III", respectively. The pattern corresponding to region "II" is composed of diffraction pots pointing to both single crystal and polycrystalline. For the area "III", only the pattern of Ge crystal was collected. Here, we attribute the diffraction rings in "I" to SEI layer observed. The SAED patterns imply the same image as the TEM analysis shown as Figure 4(c–e), both of which confirm the Li^+ migration along the inner walls. Several other low magnification imagesprovided in Figure S7 can help to understand this process. Elemental mapping can display a clearer observation upon the splitting behavior, as in Figure 5. We chose another typical unit for the EELS elemental mapping investigation. Figure 5(a) is the bright field image and Figure 5(b–d) corresponds to the C, Ge and O mapping, respectively. For EELS analysis, the low-loss of Ge results is considerable in such a thick core–shell configuration, which covers the Li-*k* edge. This type of interference makes it hard to map the real Li distribution in core–shell configuration due to the little content. Herein, the O mapping was detected to trace the electrolyte/Li^+ diffusion path based on the fact that there is no oxygen in initial GNIGTs structures and it is coexisting with Li in electrolyte/SEI layer. The muti-elements overlap image is shown in Figure 5(e), which displays a C–O–Ge sandwich structure. Noticeably, the Ge distribution map covers O rich region as shown in Figure 5(c,d). This implies the diffusion reaction occurs between Ge and electrolyte at the interface, demonstrating the formation of SEI layer here. We also

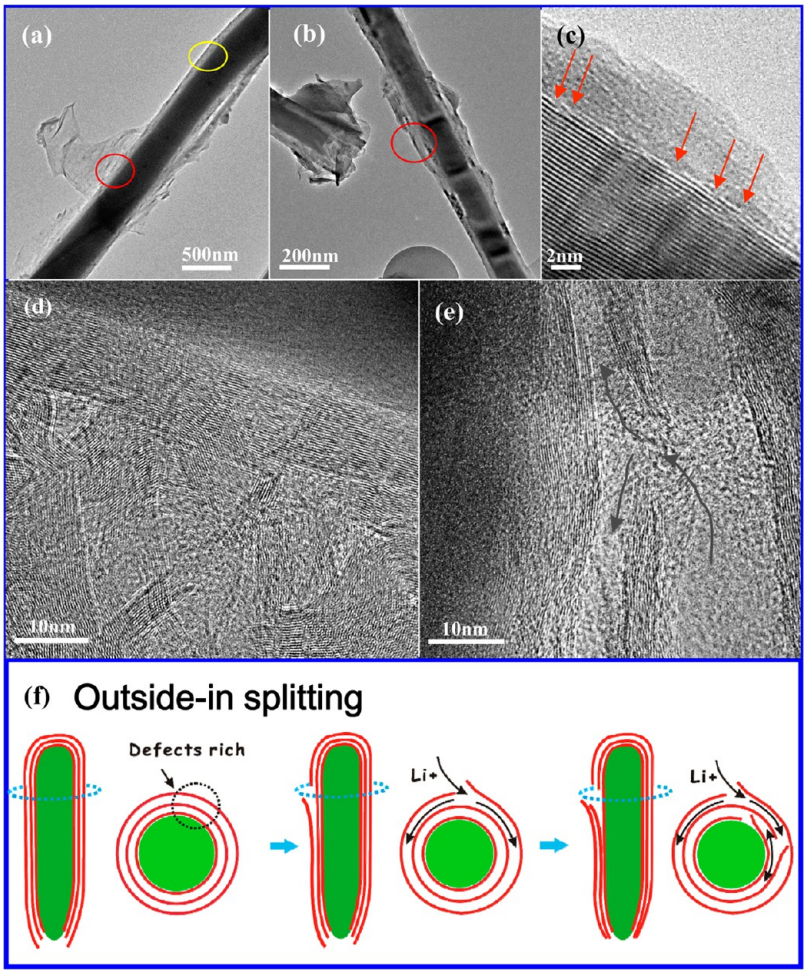

Figure 6. Outside-in splitting of the graphite shell. (a,b) Low magnification images of the units with local cracked surface with other regions remain intact. (c) The HRTEM image of the yellow circle area in (a), in which the red arrows point to the forming of defects on surface part of the graphite shell that would finally serve as Li^+ transport path. (d) The HRTEM image of splitting shell corresponding to the area marked using red circle in (a), in which the initial shell was torn into fragments of graphite sheet that adhering to the bulk. (e) The HRTEM image of splitting shell corresponding to the area marked using red circle in (b), in which the graphite shell was torn in units of several layers. The arrows display the possible penetration paths of Li^+ and the region that electrolyte can reach. (f) The illustration of the outside-in splitting mechanism, originating from the Li^+ lateral penetration effect across the defects points of carbon shell.

provide another group of EELS mapping data upon a GNIGT with thicker SEI layer in order to expose a direct Li distribution, as shown in Figure S6. The Li mapping displays a similar configuration to O distribution, although which is not clear enough due to various negative factors such as thick diameter and influence of low-loss from Ge element. However, this supplement indicates that it is reasonable to demonstrate the diffusion of Li in this case. The morphology evolution and related kinetics can be illustrated by Figure 5(g). These results demonstrate two facts: (1) the Li^+/electrolyte diffuse rapidly even along the voidless interface between the carbon shell and Ge nanowires; (2) the splitting of the carbon shell occurs due to the SEI layer forming, but not the huge expansion as a result of complete lithiation of Ge core. If we considered a single unit with a diameter of 120 nm and the SEI layer of 20 nm, the core would exhibits a volume expansion of 178% as analyzed in Figure S3, which is although insufficient to demonstrate the probability of splitting quantitatively. Additionally, the thickness statistics was provided as Figure 5(f), which was collected randomly among more than 200 nanowires. Most of the graphite shells are measured to have a thickness of 10−20 nm, although some other values are included.

Except the "zipper" cleavage, there is another type of one we called "outside-in" mechanism. By investigating the sodiation kinetics of CoS nanowires-in-CNTs with *in situ* TEM method, Su *et al.* observed the rapid diffusion of Na^+ along both the inner wall and the outer wall of the CNTs shell and found that the electrolyte may diffuse across several graphite layers through local defective sites.[32] Unlike the case of surficial transport in the *in situ* TEM investigation, the active materials here are always immersed in the electrolyte. It is obvious that the defective CNTs shell is much weaker against Li^+ insertion in this case than only relying on surficial Li^+ transport. Therefore, it is

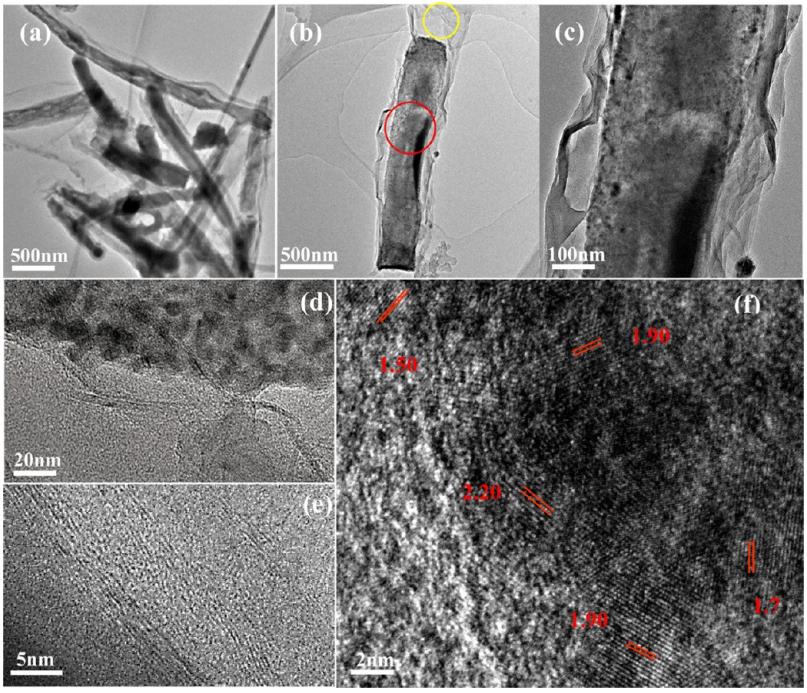

Figure 7. Characterization of the anode after the first discharge process. (a) The low magnification image of several nanowires. (b) The nanowire chosen for analysis. (c) Image in higher magnification. (d,e) The closer view of the shell morphology after the first discharge which resulted from both of the "inside-out" and "outside-in" splitting mechanism; the Ge core is still wrapped by splitting Graphite sheet. (f) The HRTEM image of the nanowire core and typical spacing are marked.

reasonable that many GNIGTs have local cracked shells as shown in Figure 6(a,b), except for the "unzipped" ones driven by SEI layer growth. Figure 6(f) illustrates the cleavage mechanism with the carbon shell splitting layer by layer in local area rich of defects. As soon as the transport paths forms by running through several layers, Li^+ would react with the inner part until the CNT shell was penetrated completely. Here in Figure 6(a,b), we picked two unites and present the change, in which the original shell were torn by the lateral diffusion of Li^+. Figure 6(c) shows the intact part of the carbon shell as marked in (a) with yellow circle. Although this section remains undestroyed, inchoate Li^+ diffusion across the layers has begun at local sites as marked using red arrows. At these points, the surficial layer exhibits high density of defects, providing rich possibilities for Li^+ insertion laterally. The red circle region displayed a splitting surface. Figure 6(d) and (e) are HRTEM images corresponding to these areas. Figure 6(d) is the closer view of the area marked in Figure 6(a) with red circle. As one can see, although half of the shell has been torn enormously, the other half still remains intact. In Figure 6(e), the original graphite shell was lifted in unit of several layers, in which mutiple paths for Li^+ transport forms, that resulted in smooth Ge−Li^+ contact. Noticeably, most of the graphite fragments are still attached to the Ge nanowire core.

Generally speaking, both of the shell splitting rules may coexist in a single nanowire hybrid. However, the outside-in cleavage contributes more and works as a predominant way for Li^+ transport during the first discharge, because it provide a relatively smooth and inevitable path for Li^+ diffusion. Actually, the splitting graphite shell plays an important part to resist the following volume expansion induced pulverization and detachment of Ge substance, as well as to enhance the Li^+/electrons migration. Figure 7 displays the typical TEM analysis of the novel structures after the first discharge procedure completely. Figure 7(a) is the low-magnification bright field image, in which obvious cracked shells and expanded nanowire cores can be seen, demonstrating the sufficient lithiation has occurred. We picked a single unit as shown in Figure 7(b) for SAED and HRTEM characterization. Figure 7(c) is the image in higher magnification. Figure S9(a) is the SAED pattern of the region marked by yellow circles, which was recorded as the reference to obtain real signal of Ge−Li alloy. Actually, the unwanted pattern was attributed to electrolyte derived compound matrix such as Li_2O. Figure S9(b) exhibits the SAED pattern of the nanowires core that was recognized to be GeLix by excluding the background signal in (d). Figure 7(c,d) is the higher magnification characterization of the nanowires surface, in which the carbon fragments in unit of several layers wrap out of the nanowire core. These data confirm that the splitting carbon shells are still in close touch with the Ge core, although the original tubes have changed a lot. Figure 7(h) is the HRTEM analysis of the Ge bulk, in which typical crystal planes have been marked.

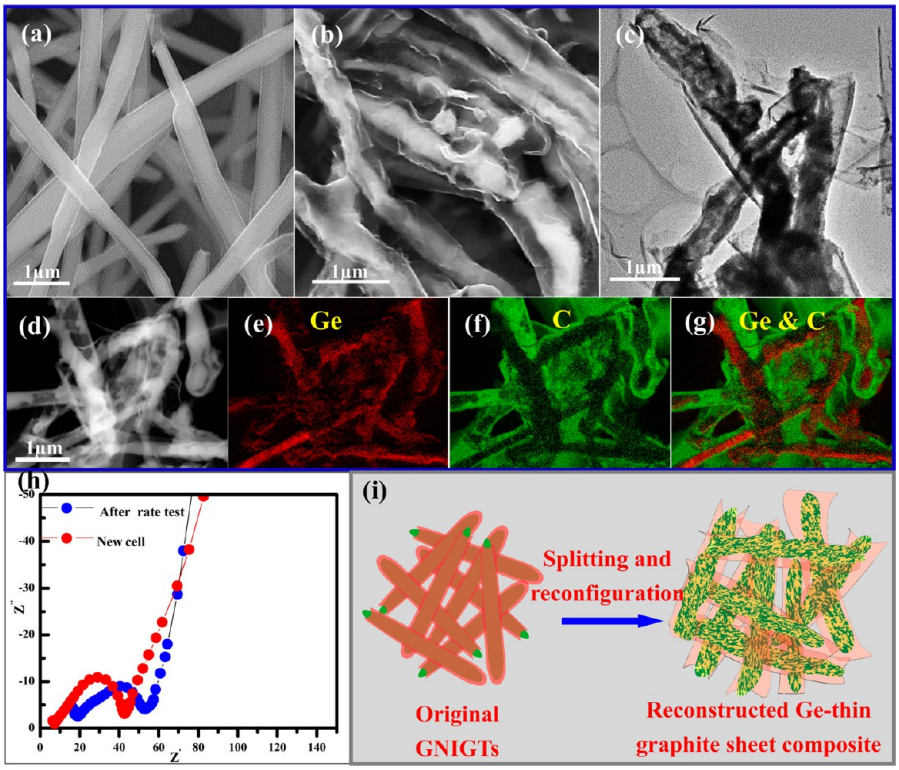

Figure 8. Structure evolution illustration and AC impedance investigation. (a) The SEM characterization of the intact anode material before lithiation reaction. (b) The SEM image of the anode after the 100th cycle; the splitting graphite shell still keeps in touch with Ge by forming a reconstructed Ge−C composite. (c) The bright field TEM image of a single unit corresponding to the sample after the 100th discharge. (d) The dark-field TEM image of several units after 100th discharge. (e-f) The EELS elemental mapping of Ge and C, respectively. (g) The overlap of Ge and C signals. (h) The AC impedance investigation of the cell; the red curve corresponds to the new device, and the blue curve is recorded after the rate test. (e) Schematic diagram of the morphological evolution of the GNGITs, displaying the alloying/dealloying resulted reconstructed effect of the novel structures.

The formed Ge−C configuration is advantageous definitely to resist volume change and to build a smooth Li^+/electrons path during the long-time work.

Moreover, cyclic voltammetry (CV) plots of the device were provided in Figure S8, which are used to demonstrate the electrochemistry Li-storage mechanism of the sample. Three cycles were tested at a scan rate of 0.1 mV/S. For the first cycle, there is a clear peak at 0.92 V, suggesting SEI film formation on surface of the graphite shell and part of the Ge nanowires. Actually, the SEI layer forms in a wide potential window because new interface between Ge and C was created continuously by unzipping the shell, just as analyzed above. The peaks locate at 0.30, 0.05 V and the peak near 0 V are related to the Li-alloying that forms different Ge−Li phases. In the second and the third cycles, stable Li^+ paths have been created. Obvious reduction peaks were detected at 0.05, 0.34, and 0.41 V, while the oxidation reactions were at 0.42 and 0.63 V. The curves demonstrated the muti-step lithiation reaction of Ge substance as reported in other works, in which several Ge−Li phases were mentioned.[20,31,33] Noticeably, although a small part of graphite shells are participant in the Li^+ insertion/exaction, we do not intend to trace that here because it contributes so little to the capacity.

Furthermore, to visualize the final morphology of the novel configuration after long cyclic process, we characterize the anode material after the 100th cycle with SEM, TEM and elemental mapping methods. Figure 8(a) is the intact GNIGTs 1D nanostructures, while Figure 8(b) displays the final morphology of the novel structures after the 100th discharge process. From Figure 8(b), after the 100th cycle, although the graphite tubes are unzipped completely, close-contact nanowires and micrographite sheet are constructed as new hybrid type. Graphite tubes derived thinner carbon sheets are still in good touch with the Ge nanowires, although the anode has experienced 100 times charge/discharge. In this new configuration, the forming quasi-2D graphite components are shared by contiguous Ge nanowires, which further preserve the nanowires from being destructed by lithiation expansion and enhance electrons/Li^+ transport. These analyses demonstrate the origin of the excellent cyclicity and rate performance of the sample. Also as displayed in Figure 8(c), there is no serious detachment of active substance on the Ge nanowires during the long-time cycles. Alternatively, porous 1D Ge architectures forms due to the repeated Li^+ insertion/extraction, which result in shorter Li^+ transport distance and enormously

increase the contact sites between Ge and electrolyte in the following cycles. On the other hand, several nanowires shown as Figure 8(d) are analyzed using EELS mapping. Figure 8(e,f) correspond to the Ge and C distribution and Figure 8(g) is the Ge/C overlap image, in which the newly formed Ge−C composite were recorded. Furthermore, more cases are provided in Figure S7. The entire process of the morphology evolution is illustrated in Figure 8(i). To gain additional insight into the cyclic behavior, the electrochemical impedance of the GNIGTs as an anode electrode was tested, as shown in Figure 8(h), in which red and blue curves correspond to the data from a new cell and the device after rate tests, respectively. Although the blue curve displays relatively larger bulk resistance and clear double charge-transfer resistance due to structural evolution during the long charge/discharge process, both curves indicate excellent charge-transfer and Li^+ diffusion behaviors. These analyses imply that the novel GNIGTs nanostructures maintain very good electric contact and smooth Li^+ transport features during the long-time cycle, demonstrating the advantages when used as anode material in LIB device.

CONCLUSIONS

In this work, by creating a solid/liquid interface between Ge and C in a CVD system, we achieved a novel design for GNIGTs in a one-step process *via* a simple, self-catalyzed, and synergetic confined growth method, in which asymmetrical graphite crystallization and a continuous supply of noneutectic Ge and C in the atmosphere drive the 1D core−shell configuration. A detailed LIB half-cell device test confirmed the excellent performance of GNIGTs as an anode material. After 100 cycles, 88.9% of the second specific capacity remained. A systematic investigation of the morphology evolution at different lithiation periods supplies a clear image of LIB kinetics and demonstrates how a ∼50-layer graphite shell contributes to the capacity and rate performance. During the repeated cycles, the graphite shells would split by inside-out and outside-in mechanism. Repeated cycles finally results in the reconstruction of the core−shell configuration by forming interesting Ge nanowires−graphite nanoribbons hybrid, which performs well to enhance the electrons/Li^+ transport.

EXPERIMENTAL SECTION

Synthesis of GNIGTs. The fabrication of the product was carried out in a CVD system equipped with a graphite heater that has been demonstrated elsewhere.[34,35] The detailed setup and process of the experiment can be described as follows. After GeO_2 powder (20 mg) was placed on one side, a ceramic chip (160 mm × 15 mm × 1 mm) was pushed into a semiclosed corundum protected tube, which was then placed in the furnace chamber with GeO_2 at the central region of the heater. The furnace was then heated stepwise to 1200 °C in 60 min and held at that temperature for 120 min. As soon as the temperature reached 400 °C, CH_4 and H_2 were introduced into the chamber at flow rates of 10 and 100 sccm, respectively, and the target pressure was 20 kPa until completion of the reaction process. Finally, the product was found at the other side of the ceramic chip, as shown in Figure 2.

Cell Assembly and Test. Electrochemical experiments were carried out in a two-electrode electrochemical cell by using lithium foil as a counter-electrode and the sample as working electrodes. The working electrodes were prepared by mixing the active material, carbon black, and polyvinylidene fluoride (PVDF) in a weight ratio of 7:2:1 in *N*-methylpyrrolidinone (NMP), which was coated uniformly on pure copper foil by an automatic thick film coater (AFA-I). The weight of the active substance is about 0.5 mg. After drying in a vacuum chamber at 120 °C for 12 h, the foil was rammed by an electromotive roller (MR-100A) and tailored to the appropriate size by a coin-type cell microtome (T-06). The final cell was fabricated using a polypropylene micromembrane as the separator (Celgard, 2400, USA); 1 M LiPF6 in ethylene carbonate (EC) and diethyl carbonate (DEC) with a weight ratio of 1:1 served as the electrolyte. Cyclic voltammetry of the cell was scanned at 0.1 mV/s in the voltage range of 0.001−2.5 V (*versus* Li/Li^+) on an Ivium electrochemical workstation. The discharge−charge measurement of the cells was carried out at room temperature using a multichannel battery tester (Shenzhen Newware Technology Limited Co., China).

Conflict of Interest: The authors declare no competing financial interest.

Acknowledgment. This work was financially supported by the National Natural Science Foundation of China (51125008, 11274392, U1401241).

Supporting Information Available: Figures S1−S10. This material is available free of charge *via* the Internet at http://pubs.acs.org.

REFERENCES AND NOTES

1. Seng, K. H.; Park, M. H.; Guo, Z. P.; Liu, H. K.; Cho, J. Self-Assembled Germanium/Carbon Nanostructures as High-Power Anode Material for the Lithium-Ion Battery. *Angew. Chem., Int. Ed.* **2012**, *51*, 5657–5661.
2. Liu, X. H.; Huang, S.; Picraux, S. T.; Li, J.; Zhu, T.; Huang, J. Y. Reversible Nanopore Formation in Ge Nanowires during Lithiation-Delithiation Cycling: An *In Situ* Transmission Electron Microscopy Study. *Nano Lett.* **2011**, *11*, 3991–3997.
3. Chan, C. K.; Zhang, X. F.; Cui, Y. High Capacity Li Ion Battery Anodes using Ge Nanowires. *Nano Lett.* **2008**, *8*, 307–309.
4. Park, M. H.; Kim, K.; Kim, J.; Cho, J. Flexible Dimensional Control of High-Capacity Li-Ion-Battery Anodes: From 0D Hollow to 3D Porous Germanium Nanoparticle Assemblies. *Adv. Mater.* **2010**, *22*, 415–417.
5. Wang, D.; Chang, Y. L.; Wang, Q.; Cao, J.; Farmer, D. B.; Gordon, R. G.; Dai, H. Surface Chemistry and Electrical Properties of Germanium Nanowires. *J. Am. Chem. Soc.* **2004**, *126*, 11602–11611.
6. Graetz, J.; Ahn, C. C.; Yazami, R.; Fultz, B. Nanocrystalline and Thin Film Germanium Electrodes with High Lithium Capacity and High Rate Capabilities. *J. Electrochem. Soc.* **2004**, *151*, A698.
7. Chan, C. K.; Cui, Y. High-Performance Lithium Battery Anodes Using Silicon Nanowires. *Nat. Nanotechnol.* **2008**, *3*, 31–35.
8. Magasinski, A.; Dixon, P.; Hertzberg, B.; Kvit, A.; Ayala, J.; Yushin, G. High-Performance Lithium-Ion Anodes Using a Hierarchical Bottom-Up Approach. *Nat. Mater.* **2010**, *9*, 353–358.
9. Evanoff, K.; Magasinski, A.; Yang, J.; Yushin, G. Nanosilicon-Coated Graphene Granules as Anodes for Li-Ion Batteries. *Adv. Energy Mater.* **2011**, *1*, 495–498.
10. Teki, R.; Datta, M. K.; Krishnan, R.; Parker, T. C.; Lu, T. M.; Kumta, P. N.; Koralkar, N. Nanostructured Silicon Anodes for Lithium Ion Rechargeable Batteries. *Small* **2009**, *5*, 2236–2242.

11. Yang, G. Z.; Song, H. W.; Cui, H.; Liu, Y. C.; Wang, C. X. Ultrafast Li-Ion Battery Anode with Superlong Life and Excellent Cycling Stability from Strongly Coupled ZnO Nanoparticle/Conductive Nanocarbon Skeleton Hybrid Materials. *Nano Energy* **2013**, *2*, 579–585.
12. Song, H. W.; Li, N.; Cui, H.; Wang, C. X. Enhanced Capability and Cyclability of SnO_2−Graphene Oxide hybrid Anode by Frmly Anchored SnO_2 Quantum Dots. *J. Mater. Chem. A* **2013**, *1*, 7558–7562.
13. Pang, C. L.; Cui, H.; Yang, G. W.; Wang, C. X. Flexible Transparent and Free-Standing Silicon Nanowires Paper. *Nano Lett.* **2013**, *13*, 4708–4714.
14. Li, N.; Song, H. W.; Cui, H.; Yang, G. W.; Wang, C. X. Self-Assembled Growth of Sn@CNTs on Vertically Aligned Graphene for Binder-Free High Li-Storage and Excellent Stability. *J. Mater. Chem. A* **2014**, *2*, 2526–2537.
15. Jin, S. X.; Li, N.; Cui, H.; Wang, C. X. Growth of the Vertically Aligned Graphene@Amorphous GeOx Sandwich Nanoflakes and Excellent Li Storage Properties. *Nano Energy* **2013**, *2*, 1128–1136.
16. Wang, B.; Li, X. L.; Zhang, X. F.; Luo, B.; Zhang, Y. B.; Zhi, L. J. Contact-Engineered and Void-Involved Silicon/Carbon Nanohybrids as Lithium-Ion-Battery Anodes. *Adv. Mater.* **2013**, *25*, 3560–3565.
17. Wang, B.; Li, X. L.; Zhang, X. F.; Luo, B.; Jin, M. H.; Liang, M. H.; Dayeh, S. A.; Picraux, S. T.; Zhi, L. J. Adaptable Silicon-Carbon Nanocables Sandwiched between Reduced Graphene Oxide Sheets as Lithium Ion Battery Anodes. *ACS Nano* **2013**, *7*, 1437–1445.
18. Lin, J.; Peng, Z. W.; Xiang, C. S.; Ruan, G. D.; Yan, Z.; Natelson, D.; Tour, J. M. 3-Dimensional Graphene Carbon Nanotube Carpet-Based Microsupercapacitors with High Electrochemical Performance. *ACS Nano* **2013**, *7*, 6001–6006.
19. Xue, D. J.; Xin, S.; Yan, Y.; Jiang, K. C.; Yin, Y. X.; Guo, Y. G.; Wan, L. J. Improving the Electrode Performance of Ge through Ge@C Core−Shell Nanoparticles and Graphene Networks. *J. Am. Chem. Soc.* **2012**, *134*, 2512–2515.
20. Li, L.; Seng, K. H.; Feng, C. Q.; Liu, H. K.; Guo, Z. P. Synthesis of Hollow GeO_2 Nanostructures, Transformation into Ge@C, and Lithium Storage Properties. *J. Mater. Chem. A* **2013**, *1*, 7666–7672.
21. Seng, K. H.; Park, M. H.; Guo, Z. P.; Liu, H. K.; Cho, J. Self-Assembled Germanium/Carbon Nanostructures as High-Power Anode Material for the Lithium-Ion Battery Angew. *Chem. Int. Ed.* **2012**, *51*, 5657–5661.
22. Zhong, C.; Wang, J. Z.; Gao, X. W.; Wexler, D.; Liu, H. K. *In Situ* One-step Synthesis of a 3D Nanostructured Germanium-Graphene Composite and Its Application in Lithium-Ion Batteries. *J. Mater. Chem. A* **2013**, *1*, 10798–10804.
23. Wang, C.; Ju, J.; Yang, Y. Q.; Tang, Y. F.; Lin, J. H.; Shi, Z. J.; Han, R. P. S.; Huang, F. Q. *In Situ* Grown Graphene-Encapsulated Germanium Nanowires for Superior Lithium-Ion Storage Properties. *J. Mater. Chem. A* **2013**, *1*, 8897–8902.
24. Seng, K. H.; Park, M.; Guo, Z. P.; Liu, H. K.; Cho, J. Catalytic Role of Ge in Highly Reversible GeO_2/Ge/C Nanocomposite Anode Material for Lithium Batteries. *Nano Lett.* **2013**, *13*, 1230–1236.
25. Liu, X. H.; Fan, F. F.; Yang, H.; Zhang, S. L.; Huang, J. Y.; Zhu, T. Self-Limiting Lithiation in Silicon Nanowires. *ACS Nano* **2013**, *7*, 1495–1503.
26. Liao, J. Y.; Higgins, D.; Lui, G.; Chabot, V.; Xiao, X. C.; Chen, Z. W. Multifunctional TiO_2−C/MnO_2 Core−Double-Shell Nanowire Arrays as High-Performance 3D Electrodes for Lithium Ion Batteries. *Nano Lett.* **2013**, *13*, 5467–5473.
27. Wu, Y.; Yang, P. Germanium/Carbon Core-Sheath Nanostructures. *Appl. Phys. Lett.* **2000**, *77*, 43–45.
28. Sutter, E.; Sutter, P. Au-Induced Encapsulation of Ge Nanowires in Protective C Shells. *Adv. Mater.* **2006**, *18*, 2583–2588.
29. Seo, M. H.; Park, M.; Lee, K. T.; Kim, K.; Kim, J.; Cho, J. High Performance Ge Nanowire Anode Sheathed with Carbon for Lithium Rechargeable Batteries. *Energy Environ. Sci.* **2011**, *4*, 425–428.
30. Liu, J.; Song, K. P.; Zhu, C. B.; Chen, C. C.; van Aken, P. A.; Maier, J.; Yu, Y. Ge/C Nanowires as High-Capacity and Long-Life Anode Materials for Li-Ion Batteries. *ACS Nano* **2014**, *8*, 7051–7059.
31. Seng, K. H.; Park, M.; Guo, Z. P.; Liu, H. K.; Cho, J. Self-Assembled Germanium/Carbon Nanostructures as High-Power Anode Material for the Lithium-Ion Battery. *Angew. Chem., Int. Ed.* **2012**, *51*, 5657–5659.
32. Su, Q. M.; Du, G. H.; Zhang, J.; Zhong, Y. J.; Xu, B. S.; Yang, Y. H.; Neupane, S.; Kadel, K.; Li, W. Z. *In Situ* Transmission Electron Microscopy Investigation of the Electrochemical Lithiation Delithiation of Individual Co_9S_8/Co-Filled Carbon Nanotubes. *ACS Nano* **2013**, *7*, 11379–11387.
33. Yoon, S.; Park, C.; Sohn, H. Electrochemical Characterizations of Germanium and Carbon-Coated Germanium Composite Anode for Lithium-Ion Batteries. *Electrochem. Solid-State Lett.* **2008**, *11*), A42.
34. Sun, Y.; Chen, Y.; Ding, C. R.; Yang, G. W.; Ma, Y. M.; Wang, C. X. One-Dimensional Al_4O_4C Ceramics: A New Type of Blue Light Emitter. *Sci. Rep.* **2013**, *3*, 1749.
35. Sun, Y.; Cui, H.; Jin, S. X.; Wang, C. X. Eutectic Solidification Applied to Nanofabrication: A Strategy to Prepare Large-Scale Tungsten Carbide Nanowalls. *J. Mater. Chem.* **2012**, *22*, 16566.